Published in IET Generation, Transmission & Distribution
Received on 8th January 2014
Revised on 27th September 2014
Accepted on 9th November 2014
doi: 10.1049/iet-gtd.2014.0024

Special Issue on Sensors and Data Analytics for Smart Grid Infrastructure

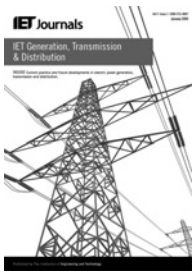

ISSN 1751-8687

Adaptive fault identification and classification methodology for smart power grids using synchronous phasor angle measurements

Pathirikkat Gopakumar[1], *Maddikara Jaya Bharata Reddy*[1], *Dusmanta Kumar Mohanta*[2]

[1]*Department of EEE, NIT, Tiruchrapallli, Tamil Nadu 620015, India*
[2]*Department of EEE, MVGR College of Engineering, Vizianagaram, Andhra Pradesh 535005, India*
E-mail: gopuvattekkat@gmail.com

Abstract: Smart power grids (SPGs) entail comprehensive real-time smart monitoring and controlling strategies against contingencies such as transmission line faults. This study proposes a novel methodology for identifying and classifying transmission line faults occurring at any location in a power grid from phasor measurement unit measurements at only one of the generator buses. The proposed methodology is based on frequency domain analysis of equivalent voltage phase angle and equivalent current phase angle at the generator bus. Equivalent voltage and current phase angles are the angles made by three-phase equivalent voltage and current phasors with respect to reference axis. These angles are estimated through Park's transformation and frequency domain analysis is performed over a fixed time span equal to inverse of system nominal frequency using fast Fourier transformation. The proposed methodology can be utilised for relaying purposes in case of single transmission lines as well as for system protection centre (SPC) applications in power grid. The significance of the fault information from the methodology is for assisting SPC in SPGs for transmission line fault detection and classification to restore the transmission lines at the earliest and initiate wide-area control actions to maintain system stability against disturbances generated by occurrence and clearance of fault.

1 Introduction

Conventional power networks across the globe are undergoing a transformation towards smart power grids (SPGs) incorporating advanced monitoring and control methodologies [1–3]. Wide-area monitoring systems based on global positioning system (GPS) assisted phasor measurement units (PMUs) is a crucial constituent of SPG [3–5] for such methodologies. PMUs perform real-time synchronised voltage and current phasor measurements, which facilitate accurate monitoring of grid dynamics in real time [6, 7]. In contrast to conventional grids, SPGs are equipped with renewable energy powered distributed generation units (DGs) and microgrids (MGs) in large scale. In contrast to conventional power grids, smart grids are equipped with renewable energy powered distributed generation units (DGs) and MGs in large scale. As a consequence, the operational behaviour of smart grids becomes diverse from that of conventional power grids [8–10]. The transmission line faults can have higher impact on operational stability of smart grids incorporated with large-scale DGs and MGs [8, 9]. After occurrence of transmission line fault in smart grid, the disturbance because of such fault can lead the MGs to switch over to islanded mode. This islanding operation can again create additional disturbance in the system which is already disturbed by the fault [8–11]. Since the system inertia of smart grids equipped with large-scale DGs and MGs is much lower than that of conventional power grids, these disturbances can initiate power oscillations and hence can affect the overall stability of the system [8–12]. Hence, it is essential to have a methodology that informs system protection centre (SPC) about the occurrence of the fault and its type. This information about the occurrence of fault and its type can enable SPC to initiate fault localisation algorithms to restore the transmission line at the earliest and initiate wide-area control actions to heal the disturbances [13, 14]. Hence, development of intelligent protection schemes for detecting and classifying transmission line faults in smart grids have received a lot of research interest in recent years.

Many fault identification and classification algorithms for transmission line protection have been reported in the literature. Major contributions are quoted here. Chanda *et al.* [15] proposed a wavelet multi-resolution analysis for fault classification in transmission lines fed from both the ends. Although the methodology can classify the type of fault, the phases involved in the fault were not discriminated. Ferrero *et al.* [16] presented a fuzzy set approach for real-time fault classification of line-to-ground (LG) and line-to-line-to-ground (LLG) faults. Wavelet-based approach for distinguishing single-phase faults from capacitor switching surges was presented in [17]. Fault classification methodology based on adaptive

neuro-fuzzy inference system (ANFIS) was proposed in [18]. The proposed methodology studied the fault classification problem considering the effect of power swing. Neural network-based fault classification method utilising the high-frequency noise generated by the fault was presented in [19]. Jaya Bharata Reddy [20] presented a real-time wavelet-fuzzy approach for fault classification. A combined approach of wavelet-neuro-fuzzy technique for digital relaying was proposed in [21]. However, majority of the fault identification and classification methods presented in the literature [15–21] are limited to specific network configurations such as transmission lines fed from one end or from double ends. Hence, they are not suitable for SPC application to detect and classify transmission line faults in power grids.

This paper proposes a novel adaptive transmission line fault identification and classification methodology based on frequency domain analysis based on equivalent voltage and current phase angles estimated using PMU measurements at any one of the generator buses in the grid. Equivalent voltage and current phasors are estimated using Park's transformation of the measured three-phase voltage and current phasors by the PMU at the generator bus. Phase angle that the three-phase equivalent voltage and current phasors establish with rotating reference frame are termed as equivalent voltage phase angle and equivalent current phase angle, respectively. These phase angles are recorded in real time and analysed through fast Fourier transform (FFT) over a time span of inverse of nominal system frequency. Frequency spectrum coefficients computed through FFT analysis are found to have the hidden information for real-time transmission line fault identification and classification. Detection of transmission line faults can be accomplished directly from the features extracted through the FFT analysis and support vector machine (SVM) has been deployed for classifying the fault detected. PMU is utilised in this paper for synchronous measurements of voltage and current phasors at the generator bus. The proposed approach has been validated through extensive case studies carried out on a standard IEEE-14 bus system modelled in MATLAB/SIMULINK environment. This paper assumes that all necessary communication facilities are available in SPG without any constraints. Results of the case studies corroborate the efficacy of the proposed methodology for real-time transmission line fault identification and classification in SPGs.

Main contribution of this paper is that the synchronous measurements of voltage and current phasors using a single PMU at any one of the generator buses are sufficient to precisely identify and classify any types of faults at any location in SPG. The fault detection and phase classification information by the proposed methodology can be used for relaying operation in single transmission lines as well as for SPC applications in power grid networks. However, significance of the proposed algorithm is to support SPC for fault localisation algorithms to restore the faulty line at the earliest. Moreover, the fault information can assist SPC to undertake necessary wide-area control actions to maintain operational stability of SPG following the transmission line faults and associated disturbances [13, 14].

2 Phasor estimation using PMU

Phasor estimation is started with sampling the original input signal at a rate of N-samples per cycle. This set of N-samples constitutes a sample window, as shown in Fig. 1. Discrete Fourier transform (DFT) is applied on this sample window to achieve the phasor form (both voltage and angle) of the signal. The concepts of phasors and phasor estimation are illustrated in depth in [6, 7].

In commercial PMUs, once 'Window-1' is taken for phasor estimation the next window taken will be 'Window-N'. The sample windows in between are omitted, so that in a 50 Hz system, a total of 50 phasors will be estimated in 1 s. All these phasors will be reported to remote location. Similarly depending on the phasor estimation rate for a specific application, the appropriate sampling windows are selected in 1 s. However, this type of phasor estimation does not yield a rotating phasor. Since, the proposed methodology necessitates a rotating phasor to extract the dynamics of the equivalent power factor angle (EPFA) during the fault, unlike commercial PMUs, the proposed methodology is utilising all the sample windows for phasor estimation (for example, starting from 'Window-1' to 'Window $N-1$') [6, 7]. However, the estimated phasors are processed locally and only fault information is sent to SPC.

3 Real-time equivalent phase angle estimation technique

Real-time estimation of equivalent voltage and current phase angles are illustrated in this section. Equivalent voltage phase angle (Δ) is the angle made by the equivalent three-phase voltage phasor (V_s) with the reference axis. Similarly the angle made by three-phase equivalent current phasor (I_s) is termed as equivalent current phase angle (Ψ).

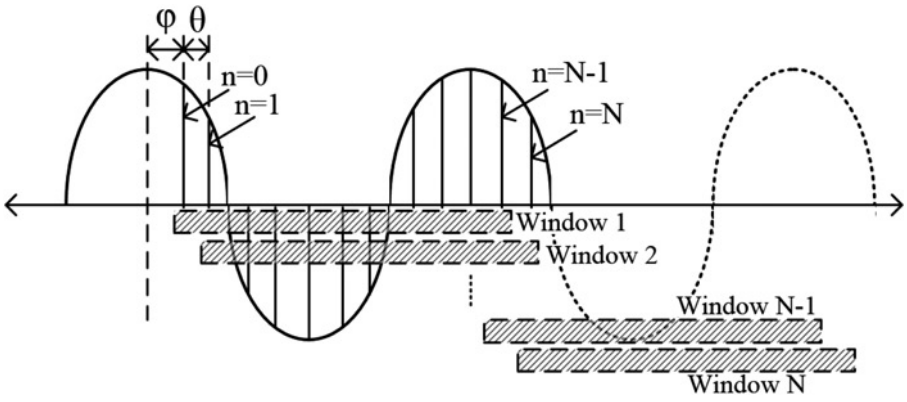

Fig. 1 *Sampling windows for phasor estimation*

IET Gener. Transm. Distrib., 2015, Vol. 9, Iss. 2, pp. 133–145
doi: 10.1049/iet-gtd.2014.0024

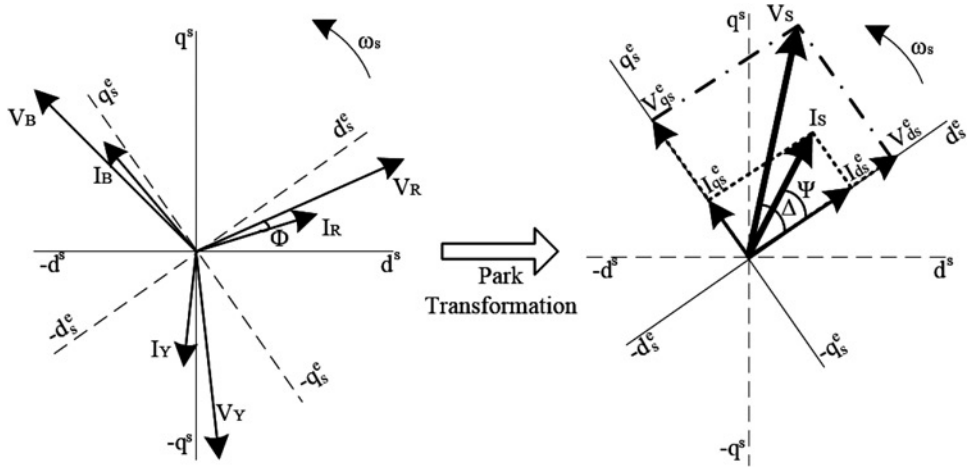

Fig. 2 *Phasor diagram of Park's transformation*

The concept of these angles is illustrated in Fig. 2. Estimations of three-phase equivalent voltage and current phasors are achieved through mapping the three-phase synchronous voltage and current phasor measurements from PMU to a reference frame rotating at nominal frequency of the grid. This mapping of three-phase quantities to equivalent two-phase orthogonal quantities is commonly termed as Park's transformation, which can be expressed mathematically as in (1)–(4) [22, 23] (see (1)–(4)), where V^e_{ds} and V^e_{qs} are the direct and quadrature axes voltages in rotating reference frame. Similarly, I^e_{ds} and I^e_{qs} stand for currents. V_{RM}, V_{YM} and V_{BM} are the peak values of phase voltages, which are equal to each other during normal operating conditions. Similarly I_{RM}, I_{YM} and I_{BM} are peak values of three-phase line currents. The angle Ø stands for power factor angle between line voltage and current. Frequencies ω and ω_s correspond to frequency in radians of three-phase voltages and rotating reference frame, respectively.

Major advantage of this transformation for fault classification is that only two-phase data are required to process for analysing three-phase system. Moreover, the power frequency components in the three-phase system become DC components after the transformation and all other frequency components appear as alternating components. This facilitates better perception of harmonic quantities in voltage and current phasors [22, 23]. The Park's transformation and the concepts of equivalent voltage and current phase angles have been illustrated with the help of phasor diagram as shown in Fig. 2.

From Fig. 2, the axes d_s and q_s represent the stationary reference frame. The axes d^e_s and q^e_s stand for an autonomous rotating reference frame rotating in counter clockwise direction at nominal frequency of the grid. This renders the reference frame to be insensitive to variations in voltage or current phasors.

The equivalent voltage phasor (V_s) and current phasor (I_s) form angles Δ and Ψ, respectively, with rotating axes d^e_s and q^e_s, which can be calculated as given in (5), (6)

$$\Delta = \tan^{-1}\left(\frac{V^e_{qs}}{V^e_{ds}}\right) \tag{5}$$

$$\Psi = \tan^{-1}\left(\frac{I^e_{qs}}{I^e_{ds}}\right) \tag{6}$$

For achieving the dynamics of these angles, voltage and current phasors have to be estimated for every sample window that consists of N number of samples of the original waveform.

$$V^e_{ds} = \frac{2}{3}\left\{V_{RM}\sin(\omega t).\sin(\omega_s t) + V_{YM}\sin\left(\omega t - \frac{2\pi}{3}\right).\sin\left(\omega_s t - \frac{2\pi}{3}\right) + V_{BM}\sin\left(\omega t + \frac{2\pi}{3}\right).\sin\left(\omega_s t + \frac{2\pi}{3}\right)\right\} \tag{1}$$

$$V^e_{qs} = \frac{2}{3}\left\{V_{RM}\sin(\omega t).\cos(\omega_s t) + V_{YM}\sin\left(\omega t - \frac{2\pi}{3}\right).\cos\left(\omega_s t - \frac{2\pi}{3}\right) + V_{BM}\sin\left(\omega t + \frac{2\pi}{3}\right).\cos\left(\omega_s t + \frac{2\pi}{3}\right)\right\} \tag{2}$$

$$I^e_{ds} = \frac{2}{3}\left\{I_{RM}\sin(\omega t - \Phi).\sin(\omega_s t) + I_{YM}\sin\left(\omega t - \Phi - \frac{2\pi}{3}\right).\sin\left(\omega_s t - \frac{2\pi}{3}\right) + I_{BM}\sin\left(\omega t - \Phi + \frac{2\pi}{3}\right).\sin\left(\omega_s t + \frac{2\pi}{3}\right)\right\} \tag{3}$$

$$I^e_{qs} = \frac{2}{3}\left\{I_{RM}\sin(\omega t - \Phi).\cos(\omega_s t) + I_{YM}\sin\left(\omega t - \Phi - \frac{2\pi}{3}\right).\cos\left(\omega_s t - \frac{2\pi}{3}\right) + I_{BM}\sin\left(\omega t - \Phi + \frac{2\pi}{3}\right).\cos\left(\omega_s t + \frac{2\pi}{3}\right)\right\} \tag{4}$$

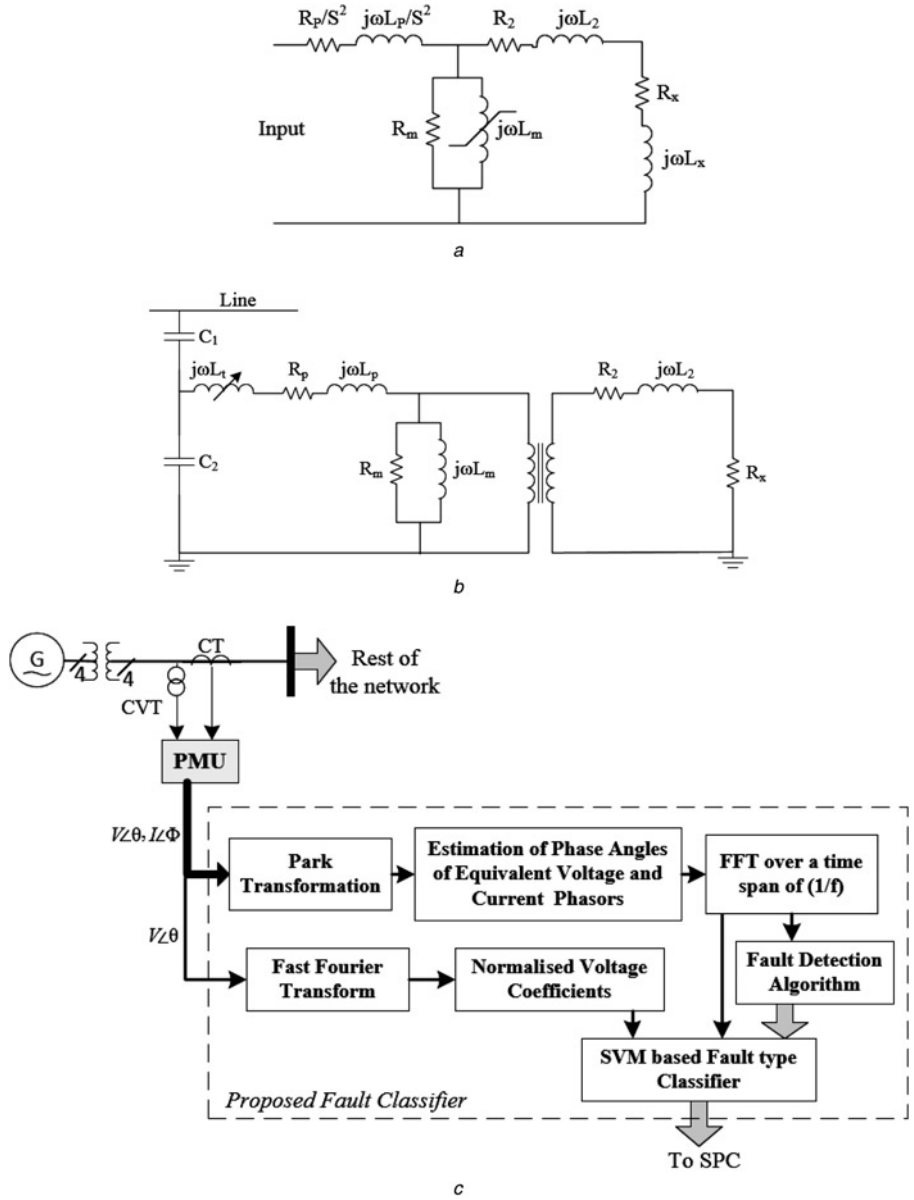

Fig. 3

a and *b* Equivalent circuits of CT and CVT, respectively
c Schematic diagram of proposed fault classification scheme

Since the axes (d_s^e and q_s^e) are rotating at nominal grid frequency, the equivalent phase angles (Δ and Ψ) have constant values during normal operating conditions. However, during transmission line faults of any type and at any location in the grid, these equivalent phase angles undergo oscillations with frequency components depending on the type of fault occurred (this is illustrated in Section 4). Frequency components present in the oscillations of equivalent phase angles (Δ and Ψ) are analysed using N-point FFT over a time span equal to inverse of nominal system frequency ($1/f$), as given in (7), (8)

$$\chi_k^{\Delta} = \left(\frac{1}{N}\right)\sum_{n=0}^{N-1}\Delta(n)\mathrm{e}^{(-2\pi kn/N)}\ 0 < k < N-1 \qquad (7)$$

$$\chi_k^{\Psi} = \left(\frac{1}{N}\right)\sum_{n=0}^{N-1}\Psi(n)\mathrm{e}^{(-2\pi kn/N)}\ 0 < k < N-1 \qquad (8)$$

The proposed methodology for real-time fault identification and classification using the frequency coefficients derived from the oscillations of equivalent phase angles has been illustrated in the following section.

4 Proposed fault identification and classification methodology

Formulation of the proposed adaptive fault identification and classification methodology based on phase angle oscillations of equivalent voltage and current phasors is illustrated here. PMU installed at generator bus estimates the voltage and current phasors from measurements from capacitor voltage transformer (CVT) and current transformer (CT), respectively. The schematic diagrams of the proposed methodology and equivalent models of CT and CVT are shown in Fig. 2.

doi: 10.1049/iet-gtd.2014.0024

4.1 CT and CVT modellings

CTs are utilised for measuring alternating currents in a line isolating the monitoring circuit from power circuit. Similarly, CVTs are employed for measuring voltages of extra high-voltage systems, where simple step down transformers are not preferred. It utilises two capacitors to split the line voltage and a transformer to provide further step down as well as isolation to the monitoring circuit. Electrical equivalent circuits of CT and CVT are given in Figs. 3*a* and *b*, respectively. All quantities in the equivalent circuit of CT are referred to the secondary side [24]. In Figs. 3*a* and *b*, R_P and L_P refer to primary winding resistance and inductance, respectively; R_2 and L_2 stand for secondary winding resistance and inductance, respectively; R_m and L_m refer to core loss components, S stands for turns ratio, L_t refers to tuning inductance, C_1 and C_2 stand for splitting capacitors and R_x and L_x refer to resistance and inductance of load connected. The proposed methodology for fault detection and classification from the CT and CVT measurements is presented in the following section.

4.2 Proposed methodology

The schematic diagram of the proposed methodology is shown in Fig. 3*c*. Equivalent voltage and current phase angles are computed from CT and CVT measurements using Park's transformation, as described in the preceding section. The equivalent phase angle waveforms are then analysed although FFT over a time span of $(1/f)$ to estimate the embedded frequency coefficients. It is observed from extensive case studies that during normal operating conditions, FFT spectrum consists of frequency coefficients corresponding to 0 Hz only and all other frequency coefficients remain at zero.

However, during fault conditions frequency coefficients corresponding to 0 and 100 Hz have severe dependency on the type of fault. The frequency coefficients corresponding to 0 Hz of equivalent voltage and current phase angle variations are represented by α_Δ and α_Ψ, respectively. The same for 100 Hz is represented as β_Δ and β_Ψ, respectively. These coefficients are calculated as given in (9)–(12)

$$\alpha_\Delta = \left(\frac{1}{N}\right)\sum_{n=0}^{N-1}\Delta(n) \tag{9}$$

$$\alpha_\Psi = \left(\frac{1}{N}\right)\sum_{n=0}^{N-1}\Psi(n) \tag{10}$$

$$\beta_\Delta = \left(\frac{1}{N}\right)\sum_{n=0}^{N-1}\Delta(n)\ \mathrm{e}^{(-200\pi n/N)} \tag{11}$$

$$\beta_\Psi = \left(\frac{1}{N}\right)\sum_{n=0}^{N-1}\Psi(n)\mathrm{e}^{(-200\pi n/N)} \tag{12}$$

Hence, the proposed fault classification methodology utilises α_Δ, α_Ψ, β_Δ and β_Ψ for real-time transmission line fault identification and classification. Fault detection algorithm based on these frequency coefficients is shown in Fig. 4.

If presence of any fault is detected, SVM classifier is utilised for classifying the type of fault. With FFT coefficients extracted, SVM classifier can classify the type of fault occurred, that is, LG or line-to-line (LL) or LLG or line-to-line-to-line (LLL). However, for discriminating the

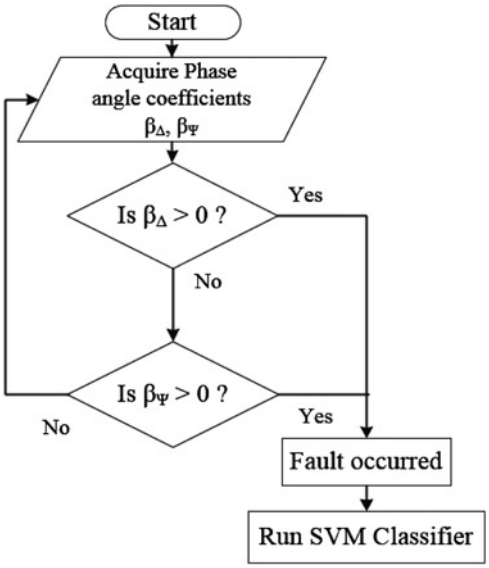

Fig. 4 *Fault detection algorithm*

phases involved in the fault, SVM classifier necessitates normalised voltage coefficients (Γ_R, Γ_Y, Γ_B) of three-phase voltages. This is because the phase information is lost once the three-phase phasors are converted to two-phase quantities using Park's transformation. Γ_R, Γ_Y and Γ_B are calculated from the FFT analysis of three-phase voltages, as given in (13)–(15)

$$\Gamma_R = \frac{P_R}{\max\{P_R,\ P_Y,\ P_B\}} \tag{13}$$

$$\Gamma_Y = \frac{P_Y}{\max\{P_R,\ P_Y,\ P_B\}} \tag{14}$$

$$\Gamma_B = \frac{P_B}{\max\{P_R,\ P_Y,\ P_B\}} \tag{15}$$

where P_i is the FFT coefficient corresponding to nominal system frequency component in the ith phase voltage. From the equivalent phase angle frequency coefficients and normalised voltage coefficients, SVM classifier classifies the type of fault occurred with phases involved. For better insight into the proposed methodology, a case study of fault condition on a transmission line fed from both the ends is considered here. The test system is represented in single line diagram as shown in Fig. 5. The transmission line considered is of 300 km long with three-phase, 400 kV generators on both sides [25]. PMUs are installed at two generator buses. In this case, phasor measurements from bus-2 have been opted for fault classification. Four types of faults are applied one at a time on the transmission line near to bus-2. Equivalent voltage and current phase angles are analysed using FFT and the frequency coefficients are

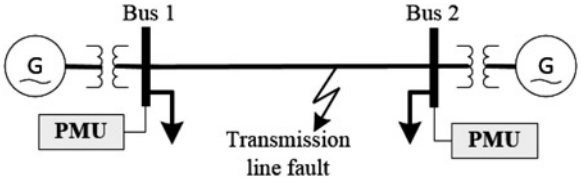

Fig. 5 *Transmission line fault in two generator system*

Table 1 FFT coefficients of equivalent phase angle variations under various operating conditions for doubly fed transmission line

Fault condition (distance, FR, FIA)	LG fault		LL fault		LLG fault		LLL fault		No fault	
	$\Delta(\alpha_\Delta, \beta_\Delta)$	$\Psi(\alpha_\Psi, \beta_\Psi)$	$\Delta(\alpha_\Delta, \beta_\Delta)$	$\Psi(\alpha_\Psi, \beta_\Psi)$	$\Delta(\alpha_\Delta, \beta_\Delta)$	$\Psi(\alpha_\Psi, \beta_\Psi)$	$\Delta(\alpha_\Delta, \beta_\Delta)$	$\Psi(\alpha_\Psi, \beta_\Psi)$	$\Delta(\alpha_\Delta, \beta_\Delta)$	$\Psi(\alpha_\Psi, \beta_\Psi)$
10 km, 0 Ω, 0°	1.62, 7.71	1.22, 0.47	0.09, 20.03	1.21, 0.43	1.01, 18.01	1.62, 0.13	0.62, 0.1	1.99, 0.1	0.182, 0	0.212, 0
50 km, 10 Ω, 15°	1.6, 7.52	1.20, 0.44	0.08, 20	1.20, 0.44	1, 18	1.6, 0.12	0.6, 0.1	1.96, 0.1		
75 km, 20 Ω, 20°	1.6, 7.52	1.19, 0.44	0.08, 20.02	1.21, 0.43	1, 18	1.6, 0.12	0.6, 0.1	1.96, 0.1		
110 km, 30 Ω, 35°	1.59, 7.64	1.19, 0.43	0.08, 20.01	1.19, 0.43	0.99, 18	1.58, 0.11	0.59, 0.1	1.95, 0.1		
150 km, 40 Ω, 60°	1.57, 6.19	1.24, 0.23	0.07, 19.86	1.20, 0.33	0.94, 17.57	1.59, 0.12	0.56, 0.1	1.94, 0.09		
175 km, 50 Ω, 80°	1.51, 5.61	1.13, 0.29	0.07, 18.03	1.10, 0.29	0.90, 15.22	1.52, 0.09	0.51, 0.09	1.78, 0.09		
200 km, 60 Ω, 90°	1.51, 5.22	1.08, 0.25	0.06, 17.17	1.05, 0.22	0.86, 14.92	1.5, 0.08	0.48, 0.09	1.77, 0.09		
210 km, 70 Ω, 110°	1.50, 5.19	1.07, 0.23	0.06, 16.96	1.04, 0.13	0.84, 14.17	1.49, 0.06	0.46, 0.08	1.74, 0.09		
250 km, 80 Ω, 120°	1.49, 5.08	1.06, 0.2	0.05, 16.01	1.01, 0.09	0.81, 14.01	1.42, 0.05	0.45, 0.08	1.72, 0.09		
275 km, 90 Ω, 140°	1.52, 7.68	1.18, 0.43	0.08, 20.01	1.19, 0.41	0.99, 18	1.58, 0.11	0.59, 0.08	1.95, 0.09		
275 km, 100 Ω, 160°	1.52, 7.88	1.17, 0.40	0.08, 19.54	1.10, 0.34	0.99, 18	1.54, 0.11	0.52, 0.07	1.93, 0.08		

tabulated in Table 1. It can be observed from Table 1 that the frequency coefficients of equivalent voltage and current phase angles are related to the type of fault which has occurred. Moreover, the coefficients are found to be insensitive to fault inception angle (FIA) and show minor variations with fault location and fault resistance (FR).

4.3 SVM-based fault classifier

SVM is one of the prevalent machine intelligence techniques for fault classification in power systems [26–31]. Multiclass SVM with one-step method has been deployed in this paper for classifying the faults from frequency coefficients of equivalent phase angle variations and normalised voltage coefficients. A detailed illustration of multiclass SVMs are available in the literature [28–31]. The classification problem can be represented as (16) [28–31]

$$\begin{aligned} &\min_{w,b,\xi} \frac{1}{2}\sum_{m=1}^{n} w_m^{\mathrm{T}} w_m + C\sum_{j=1}^{l}\sum_{m\neq y_i} \xi_i^m \\ &\text{S.T.} \quad w_{y_i}^{\mathrm{T}}\varphi(x_i) + b_{y_i} \geq w_m^{\mathrm{T}}\varphi(x_i) + b_m + 2 - \xi_i^m \\ &\xi_i^m \geq 0, \quad i = 1, \ldots, l, \quad m \in \{1, \ldots, n\}\backslash y_i \end{aligned} \tag{16}$$

The training data (x_i, y_i) have been categorised with fault type or no-fault labels. The set of equivalent phase angle coefficients (α_Δ, β_Δ, α_Ψ and β_Ψ) and normalised three-phase voltage coefficients forms the input data set for SVM classifier. The labelled fault type data corresponding to each set of values in input data set constitutes the output data set for SVM classifier. SVM classifier is trained with 1300 data sets to afford enhanced boundary for fault classification. The input data sets are generated for different fault locations, FRs and inception angles. The proposed fault classification methodology has been implemented in MATLAB/SIMULINK environment with LIBSVM toolbox for SVM training and testing [32]. Radial basis function has been utilised as the kernel function which is defined as (17) [28–31]. Kernel parameter 'γ' has been computed using grid search method based on the training data [31]

$$K\left(x_i, x_j\right) = \exp\left(-\gamma x_i - x_j\right)^2, \ \gamma > 0 \tag{17}$$

Results of the case studies are discussed in the following section.

5 Results and discussion

The proposed adaptive fault identification and classification scheme has been validated through extensive simulation studies using standard IEEE-14 bus system and results of the case study are discussed in this section. This section has been arranged as follows; the details of the IEEE-14 bus system considered for case study are presented in Section 4.1. Equivalent voltage and current phase angle variations during various transmission line faults and corresponding FFT spectra are discussed in Section 4.3. Proposed methodology for fault detection and classification is deliberated in Section 4.3. Superiority of SVM classifiers over other popular artificial intelligence methods is also validated in the section. Section 4.4 outlines a comparative study to demonstrate the supremacy of the proposed fault classification methodology over conventional approach.

5.1 IEEE-14 bus system

The IEEE-14 bus system has been modelled in MATLAB/SIMULINK environment, the single line diagram of which is given in Fig. 6. The generators and transmission line ratings considered in the IEEE-14 bus network model are as follows. Both generators are of three-phase 400 kV (LL) having positive sequence impedance of $(0.45 + 0.5\mathrm{j}\ \Omega)$ and zero sequence impedance of $(0.675 + 0.75\mathrm{j}\ \Omega)$. The three-phase transmission line is having positive and

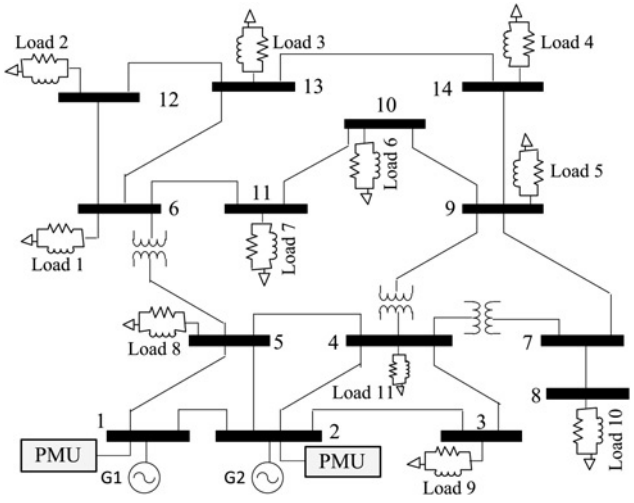

Fig. 6 *Single line diagram of IEEE-14 bus system*

doi: 10.1049/iet-gtd.2014.0024

Table 2 Length of transmission lines used in IEEE-14 bus system

Sl. no.	Branch number (bus–bus)	Length, km	Sl. no.	Branch number (bus–bus)	Length, km	Sl. no.	Branch number (bus–bus)	Length, km
1	1–2	200	8	4–7	190	15	7–9	85
2	1–5	200	9	4–9	95	16	9–10	110
3	2–5	90	10	5–6	180	17	9–14	165
4	2–4	175	11	6–12	75	18	10–11	70
5	2–3	200	12	6–13	80	19	12–13	200
6	3–4	75	13	6–11	180	20	13–14	60
7	4–5	200	14	7–8	70			

negative sequence values of resistance, inductance and capacitance as 2.34 Ω, 95.10 mH and 1.24 μF per phase per 100 km, respectively. The zero sequence values of the same parameters for the transmission line are given by 38.85 Ω, 325.08 mH and 0.845 μF per phase per 100 km, respectively [18]. Lengths of the transmission lines assumed in the developed model are tabulated in Table 2. Load connected to the buses in the network are depicted in Table 3 in terms of active and reactive power ratings.

5.2 Equivalent voltage and current phase angle variations

Equivalent voltage and current phase angles at generator-1 (G1) in IEEE-14 bus system are computed from PMU measurements at bus-1 using Park's transformation as deliberated in the preceding section. Influence of power system operating conditions on these angles is illustrated in this section. Three case studies are performed to substantiate the frequency spectra characteristics in equivalent phase angle variation caused by transmission line faults. Case-i, case–ii and case-iii correspond to normal operating conditions, sudden load changes and occurrence of transmission line faults, respectively.

Equivalent phase angles of G1 and corresponding frequency spectra for normal operating conditions are illustrated in Fig. 7. Plots of equivalent voltage phase angle and corresponding frequency spectra are given in Figs. 7*a* and *b*, respectively. Similarly equivalent current phase angle and corresponding frequency spectra are illustrated in Figs. 7*c* and *d*, respectively. Magnitudes of the FFT coefficients for equivalent voltage and current phase angles are represented by |Delta| and |Psi|, respectively, in the frequency spectra. The FFT is applied only to the data taken during fault time over a time span of inverse of nominal system frequency ($1/f$), that is, data collected over 20 ms (for 50 Hz system). This is sufficient for fault detection and classification. A sampling frequency of 10 kHz has been opted in the study, which deliver adequate accuracy in the case studies. It is observed from Figs. 7*a* to *d* that the equivalent phase angles have constant values during normal operating conditions and they are reflected as a high value for 0 Hz in frequency spectra. Case-ii has been carried out by addition of a load of 7.94 pu in bus-3 at 0.06 s and islanding loads of 6.14 pu in bus-9 at 0.07 s, 7.86 pu in bus-5 at 0.076 s, 5.98 pu in bus-8 at 0.08 s. Influence of the load change in equivalent phase angles and corresponding frequency spectra for G1 are illustrated in Figs. 8*a–d*. It is obvious from Figs. 8*a* to *d* that, although equivalent phase angle variations are resulted by the sudden load changes, frequency spectra remain unaltered in terms of frequency components present in the spectra.

For analysing case-iii, various faults of LG-fault, LL-fault, LLG-fault and LLL-fault are considered one at a time in branch 4–5 at a location of 50 km from bus-4. Equivalent phase angle variations and corresponding frequency spectra for G1 during LG-fault are shown in Figs. 9*a–d*, respectively. The same for other faults, namely, LL, LLG and LLL faults are plotted in Figs. 10–12, respectively. From Figs. 9 to 12, it can be observed that frequency components present during transmission line faults are different from that of normal operating conditions and sudden load changes. Moreover, the magnitude of the frequency components in the frequency spectra varies with the type of transmission line fault occurred. The magnitude of the frequency components extracted through FFT has been utilised for real-time fault detection and classification. Case studies conducted for detection and classification of faults in IEEE-14 bus system have been discussed in the following section.

5.3 Detection and classification of transmission line faults with the proposed methodology

Results of the case studied conducted on IEEE-14 bus system for fault detection and classification are given in Table 4. PMU measurements from bus-1 have been chosen for case study. Detection of faults can be done directly from the frequency coefficients 'α' and 'β' of equivalent voltage and current phase angle variations of generator $G1$ at bus-1. As an extension to the faults in transmission lines, bus bar faults are also studied and results are included in Table 4. FFT coefficients along with normalised voltage coefficients

Table 3 Connected load in each bus of IEEE-14 bus system

Sl. no.	Bus number	Load connected, MW, MVA	Sl. no.	Bus number	Load connected, MW, MVA	Sl. no.	Bus number	Load connected, MW, MVA
1	Bus-1	no load	6	Bus-6	53, 2.5	11	Bus-11	61, 15.1
2	Bus-2	no load	7	Bus-7	66, 15.1	12	Bus-12	74, 12.2
3	Bus-3	50, 2.5	8	Bus-8	70, 16.2	13	Bus-13	52, 9.1
4	Bus-4	73, 12.2	9	Bus-9	82, 19.5	14	Bus-14	21, 1.2
5	Bus-5	56, 9.1	10	Bus-10	75, 19			

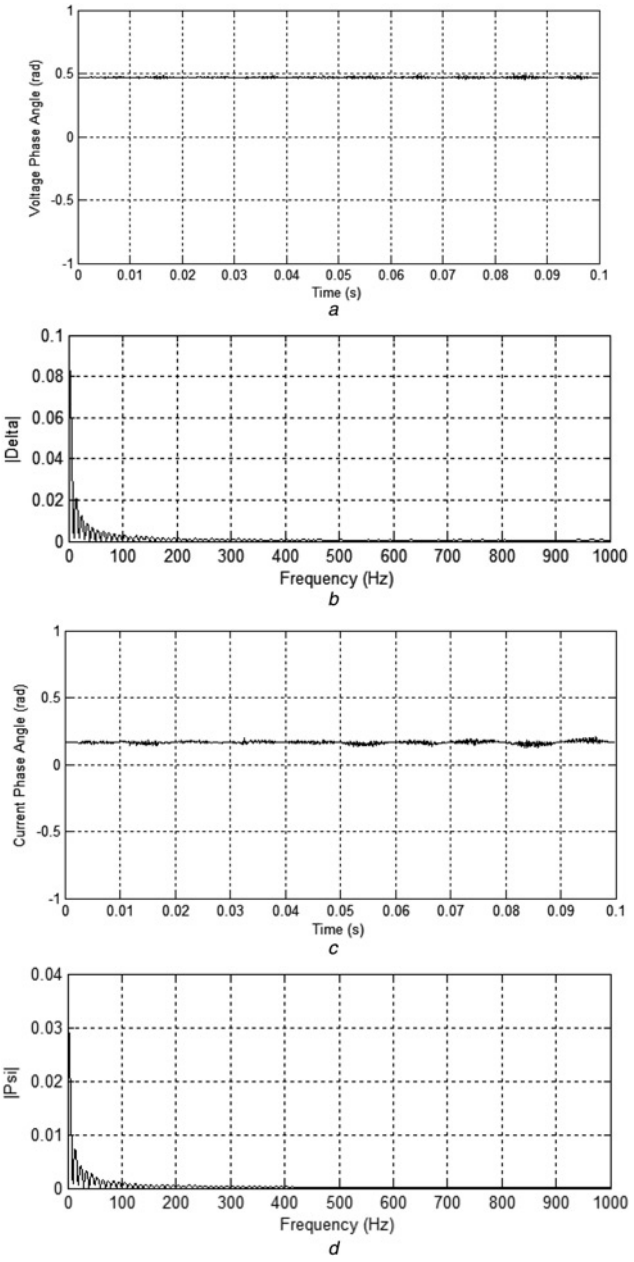

Fig. 7 *In IEEE-14 bus system, during normal operating conditions*

a Equivalent voltage phase angle variation
b FFT of equivalent voltage phase angle variation
c Equivalent current phase angle variation
d FFT of equivalent current phase angle variation

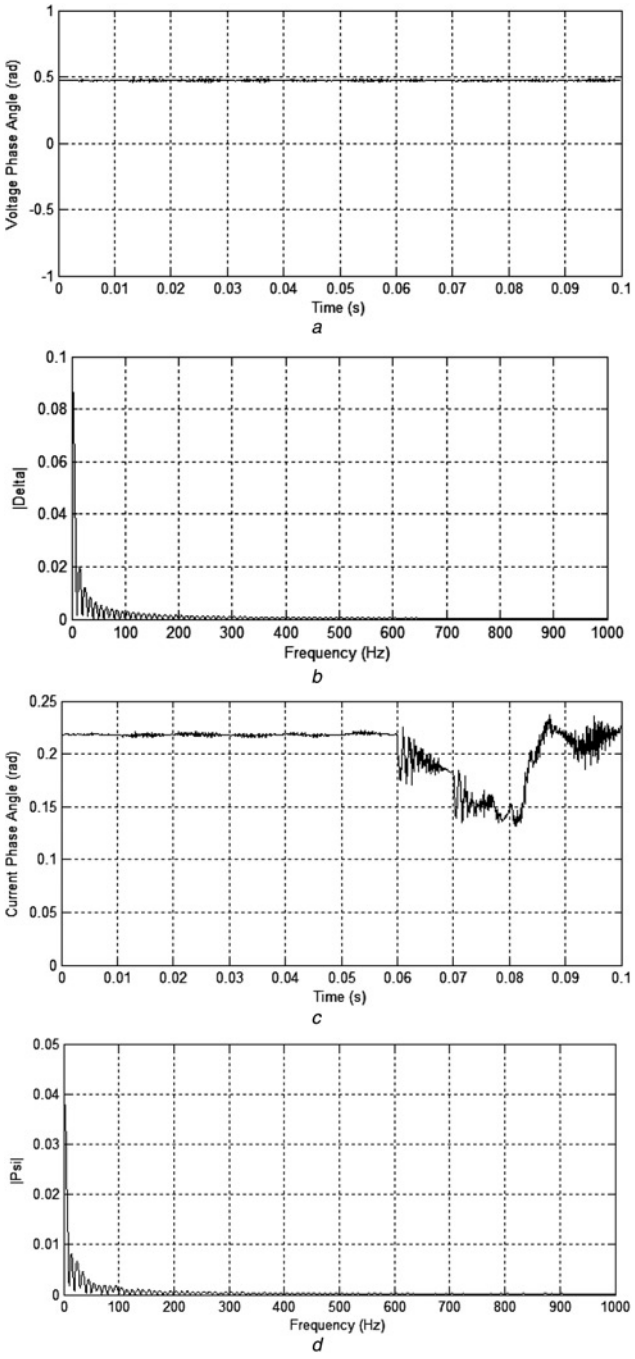

Fig. 8 *In IEEE-14 bus system, during sudden load change condition*

a Equivalent voltage phase angle variation
b FFT of equivalent voltage phase angle variation
c Equivalent current phase angle variation
d FFT of equivalent current phase angle variation

are fed to SVM classifier to classify the fault and the classification technique is shown in Fig. 13. An input–output data set comprising of 1300 samples has been utilised for training the SVM classifier. For a comparative analysis with SVM, classification has been studied with other intelligence methods such as artificial neural network (ANN) and ANFIS. The results of the case studies are included in Table 4. Details of the comparative study are given in following section.

5.3.1 Comparative study to validate the superiority of SVM over other intelligent methods: Superiority of SVM classifier for the proposed fault classification methodology has been analysed with the help of comparative study with ANN and ANFIS. The same data set of input–output patterns utilised for SVM classifier is employed for training ANN and ANFIS. Feed-forward back propagation method has been used for training ANN [33]. Hybrid optimisation method has been used for training fuzzy inference system in ANFIS network [18]. Both the networks are trained and tested using MATLAB toolbox. The classification results tabulated in Table 4 show that ANN classified all LL faults and LLL faults, but misclassified LG and LLG faults. In the case of ANFIS, all transmission line faults except LLG faults are classified accurately. This validates the superiority of SVM-based classifiers over ANN and ANFIS for the proposed fault classification methodology.

doi: 10.1049/iet-gtd.2014.0024

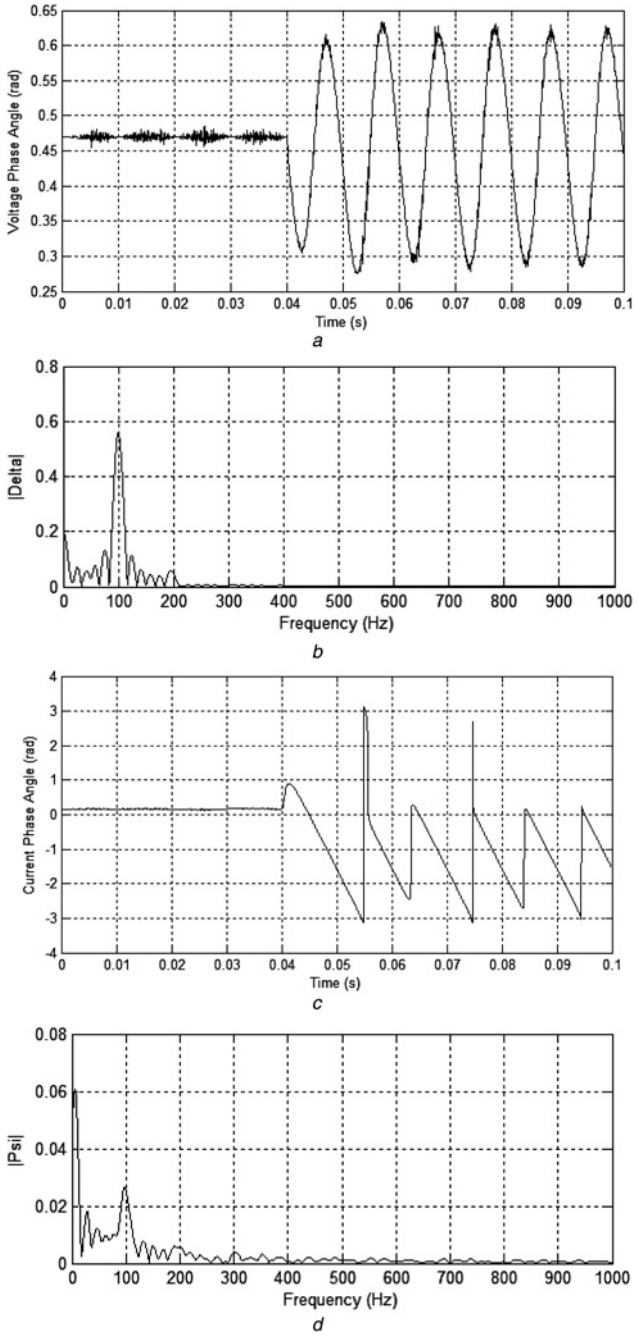

Fig. 9 *In IEEE-14 bus system, during LG-fault condition at branches 4-5, 50 km away from bus-4*

a Equivalent voltage phase angle variation
b FFT of equivalent voltage phase angle variation
c Equivalent current phase angle variation
d FFT of equivalent current phase angle variation

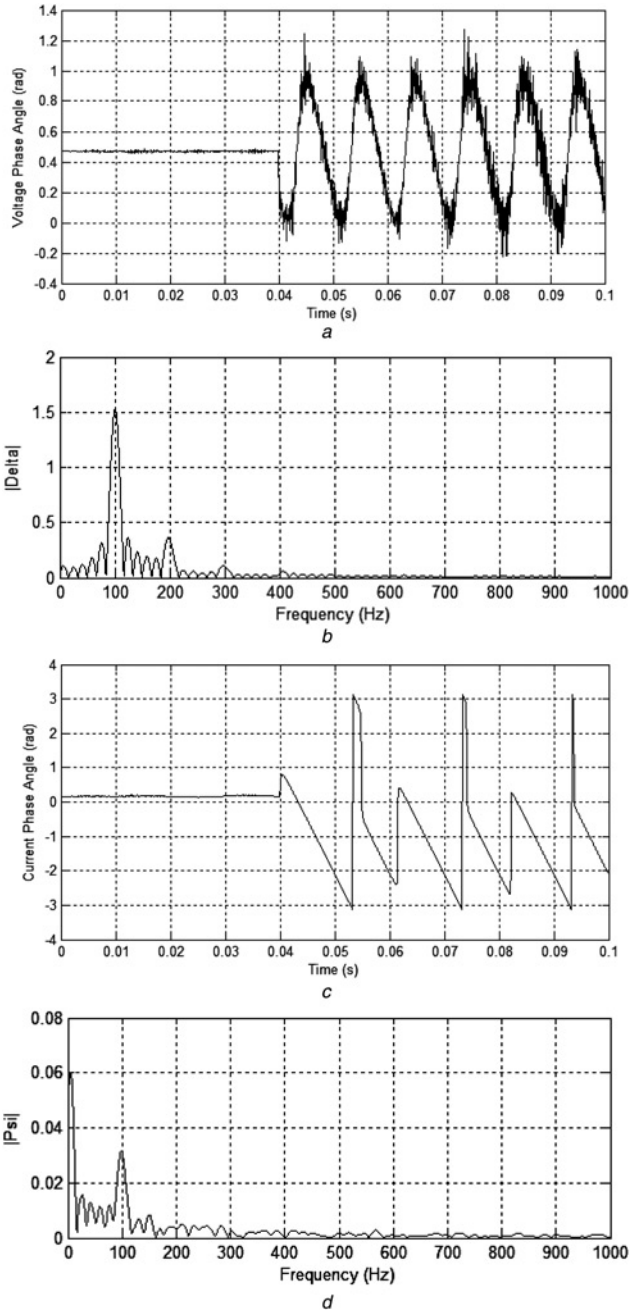

Fig. 10 *In IEEE-14 bus system, during LL fault condition at branches 4-5, 50 km away from bus-4*

a Equivalent voltage phase angle variation
b FFT of equivalent voltage phase angle variation
c Equivalent current phase angle variation
d FFT of equivalent current phase angle variation

5.4 Comparative study with existing methodology

Comparative study of the proposed methodology with a popular conventional approach is given in this section. In conventional approached for power system relaying, relative phase angle relationship between the negative and zero sequence fault currents has been utilised by many protective relays for fault detection and classification [34]. However, such an approach is limited to detection and classification of faults in a single transmission line. For detecting and classifying faults in a power grid network, relays are to be employed in all transmission lines in the network. In contrast to this, the proposed methodology can detect and classify faults occurring at any point in the grid using measurements from only one generator bus using a PMU. The methodology does not require any data from other buses or PMUs. The fault detection and classification is achieved locally at the generator bus, so that fault information alone can be sent to SPC.

5.5 Necessity of PMU for the proposed methodology

The proposed methodology utilises frequency coefficients pertaining to equivalent voltage and current phase angle

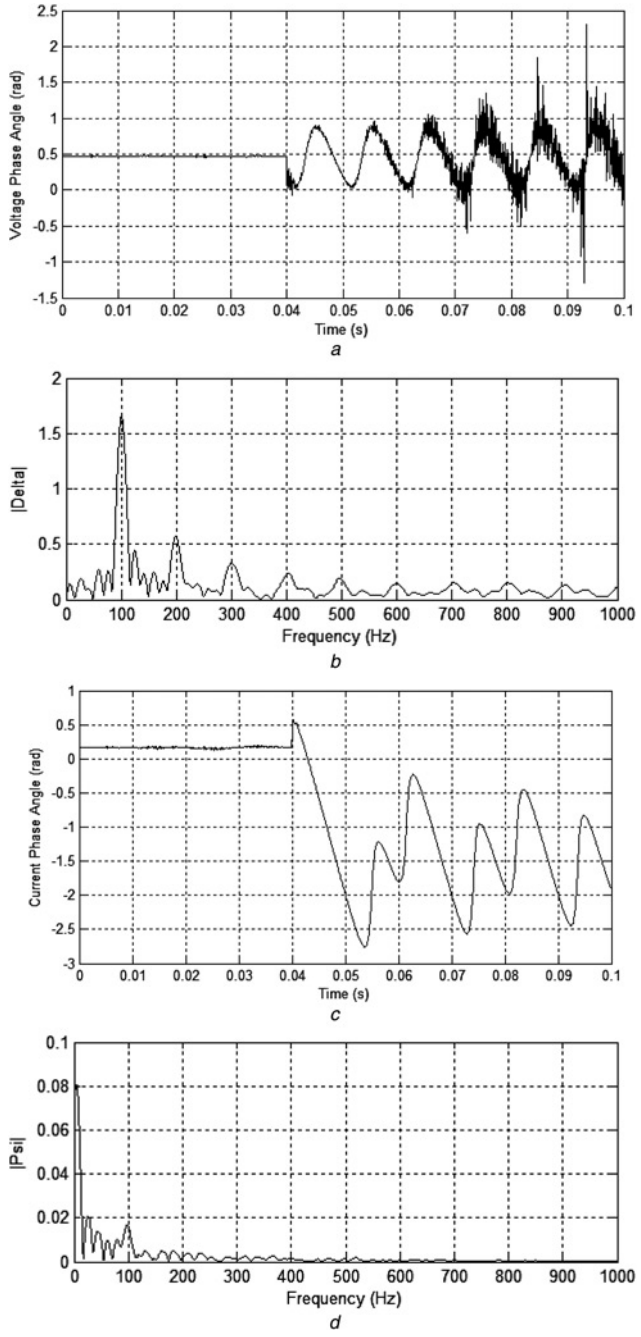

Fig. 11 *In IEEE-14 bus system, during LLG-fault condition at branches 4-5, 50 km away from bus-4*

a Equivalent voltage phase angle variation
b FFT of equivalent voltage phase angle variation
c Equivalent current phase angle variation
d FFT of equivalent current phase angle variation

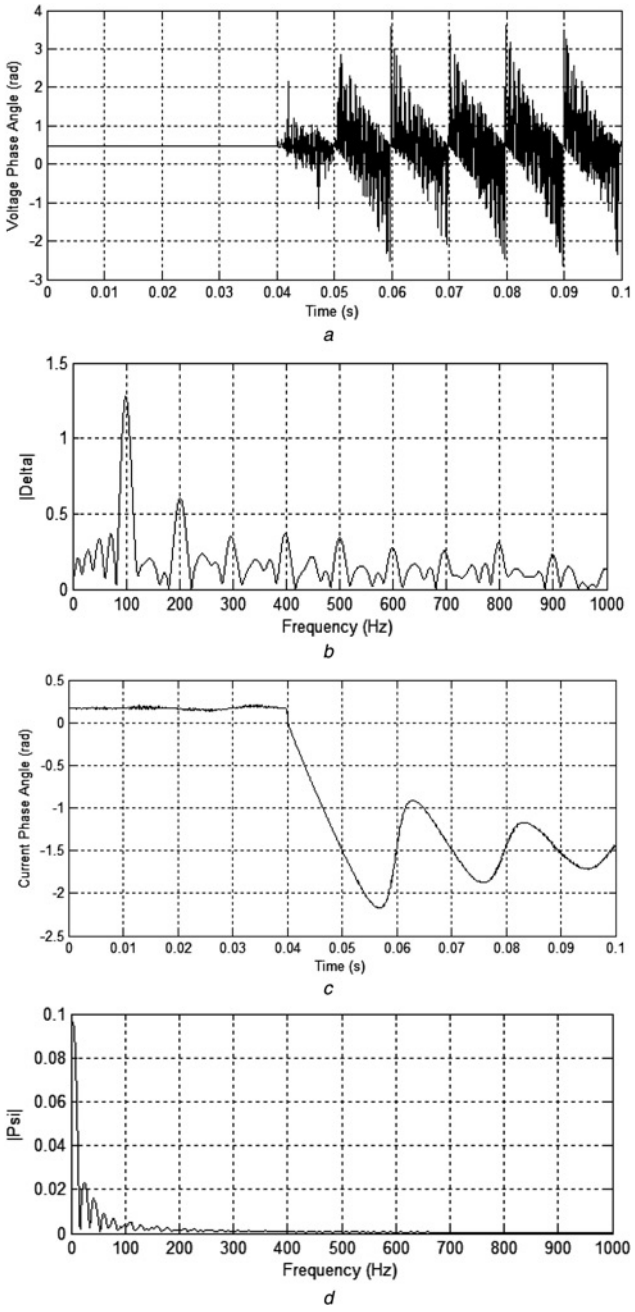

Fig. 12 *In IEEE-14 bus system, during LLL fault condition at branches 4-5, 50 km away from bus-4*

a Equivalent voltage phase angle variation
b FFT of equivalent voltage phase angle variation
c Equivalent current phase angle variation
d FFT of equivalent current phase angle variation

variations during the fault duration (as described in the preceding sections). This necessitates synchronised measurement of voltage and current phasors at single generator bus. In other words, the method needs synchronous measurements of voltage and current phasors at the generator bus. This can be achieved using a PMU, which stylises synchronised sampling of its voltage and current waveforms for phasor estimations.

If the equivalent phase angles are estimated from voltage and current phasors estimated at different instances of time, the frequency coefficients of the both cannot be correlated for fault classification. To validate the requirement of synchronous measurement of voltage and current phasors, the case study conducted for IEEE-14 bus system (Table 4) has been studied with current samples acquired at different instances from those of voltage samples (i.e. asynchronous measurements of voltage and current phasors). It is assumed that voltage samples are acquired at a time instant '$t1$' and current samples are acquired at a time instant '$t2$'. Then (1)–(4) can be written as (18)–(21) (see (18)–(21) at the bottom of next page).

Using (18)–(21), the angles Δ and Ψ are estimated and analysed using FFT over a time span of inverse of system nominal frequency (i.e. 20 ms for 50 Hz system). The FFT

doi: 10.1049/iet-gtd.2014.0024

Table 4 FFT coefficients of equivalent voltage and current phase angle variations under various operating conditions in IEEE-14 bus system

Sl. no.	Fault location	Fault type	Δ (α_Δ, β_Δ)	Ψ (α_Ψ, β_Ψ)	Υ_R, Υ_Y, Υ_B	ANN-based approach	ANFIS-based approach	SVM-based classifier
1	branches 2–4, 60 km from bus-2	AG	0.17, 0.49	0.04, 0.02	0.73, 1, 0.99	CA	AG	AG
2	branches 4–5, 50 km from bus-4	BG	0.20, 0.56	0.06, 0.02	0.99, 0.68, 1	AB	BG	BG
3	branches 1–2, 70 km from bus-1	CG	0.18, 0.44	0.04, 0.02	1, 0.99, 0.74	BC	CG	CG
4	branches 3–4, 20 km from bus-3	AB	0.05, 1.32	0.05, 0.03	0.76, 0.77, 1	AB	AB	AB
5	branches 13–14, 10 km from bus-13	BC	0.01, 0.9	0.06, 0.02	1, 0.84, 0.84	BC	BC	BC
6	branches 6–11, 40 km from bus-6	CA	0.02, 0.69	0.05, 0.02	0.84, 1, 0.85	CA	CA	CA
7	branches 12–13, 90 km from bus-12	ABG	0.11, 0.64	0.07, 0.01	0.79, 0.81, 1	AB	*AG*	ABG
8	branches 7–9, 80 km from bus-7	BCG	0.14, 0.80	0.07, 0.01	1, 0.78, 0.72	BC	*BG*	BCG
9	branches 4–9, 10 km from bus-4	CAG	0.13, 0.74	0.07, 0.01	0.77, 1, 0.73	AC	*CG*	CAG
10	branches 9–10, 30 km from bus-6	ABC	0.11, 0.12	0.08, 0.1	1, 1, 1	ABC	ABC	ABC
11	bus-3	AG	0.22, 0.53	0.05, 0.02	0.73, 1, 0.99	CA	AG	AG
12	bus-4	BG	0.24, 0.59	0.07, 0.02	0.99, 0.72, 1	AB	BG	BG
13	bus-5	CG	0.20, 0.48	0.06, 0.02	1, 0.99, 0.73	BC	CG	CG
14	bus-6	AB	0.07, 1.94	0.07, 0.04	0.68, 0.67, 1	AB	AB	AB
15	bus-7	BC	0.04, 0.9	0.08, 0.02	1, 0.66, 0.65	BC	BC	BC
16	bus-8	CA	0.05, 1.29	0.07, 0.02	0.64, 1, 0.65	CA	CA	CA
17	bus-9	ABG	0.21, 0.82	0.09, 0.03	0.69, 0.72, 1	AB	AG	ABG
18	bus-10	BCG	0.23, 0.92	0.08, 0.02	1, 0.72, 0.72	BC	BG	BCG
19	bus-11	CAG	0.14, 0.88	0.09, 0.01	0.71, 1, 0.73	AC	CG	CAG
20	bus-14	ABC	0.15, 0.17	0.1, 0.1	1, 1, 1	ABC	ABC	ABC

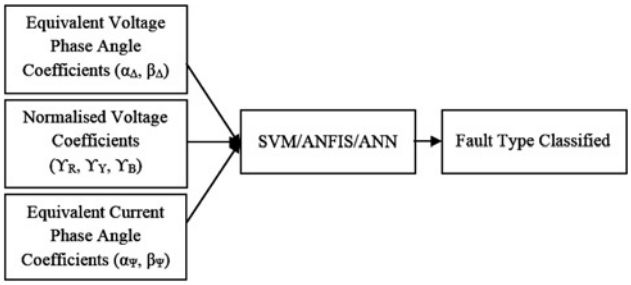

Fig. 13 *Fault classification technique*

coefficients α_Δ, β_Δ, α_Ψ and β_Ψ are given below in Table 5, along with classification results by SVM classifier. It is obvious from the results in Table 5 that SVM classifier has misclassified all the faults.

From the above result, it is very clear that asynchronous measurement of voltage and current phasors can detect the occurrence of fault, however failed to accurately classify the fault. Hence, PMU is essential to achieve synchronous measurement of voltage and current phasors to properly classify the fault occurred anywhere in the grid from a single generator bus measurement.

$$V_{ds}^{e} = \frac{2}{3}\left\{V_{\mathrm{RM}}\sin(\omega t_1).\sin(\omega_s t) + V_{\mathrm{YM}}\sin\left(\omega t_1 - \frac{2\pi}{3}\right).\sin\left(\omega_s t - \frac{2\pi}{3}\right) + V_{\mathrm{BM}}\sin\left(\omega t_1 + \frac{2\pi}{3}\right).\sin\left(\omega_s t + \frac{2\pi}{3}\right)\right\} \quad (18)$$

$$V_{qs}^{e} = \frac{2}{3}\left\{V_{\mathrm{RM}}\sin(\omega t_1).\cos(\omega_s t) + V_{\mathrm{YM}}\sin\left(\omega t_1 - \frac{2\pi}{3}\right).\cos\left(\omega_s t - \frac{2\pi}{3}\right) + V_{\mathrm{BM}}\sin\left(\omega t_1 + \frac{2\pi}{3}\right).\cos\left(\omega_s t + \frac{2\pi}{3}\right)\right\} \quad (19)$$

$$I_{ds}^{e} = \frac{2}{3}\left\{I_{\mathrm{RM}}\sin(\omega t_2 - \Phi).\sin(\omega_s t) + I_{\mathrm{YM}}\sin\left(\omega t_2 - \Phi - \frac{2\pi}{3}\right).\sin\left(\omega_s t - \frac{2\pi}{3}\right) + I_{\mathrm{BM}}\sin\left(\omega t_2 - \Phi + \frac{2\pi}{3}\right).\sin\left(\omega_s t + \frac{2\pi}{3}\right)\right\} \quad (20)$$

$$I_{qs}^{e} = \frac{2}{3}\left\{I_{\mathrm{RM}}\sin(\omega t_2 - \Phi).\cos(\omega_s t) + I_{\mathrm{YM}}\sin\left(\omega t_2 - \Phi - \frac{2\pi}{3}\right).\cos\left(\omega_s t - \frac{2\pi}{3}\right) + I_{\mathrm{BM}}\sin\left(\omega t_2 - \Phi + \frac{2\pi}{3}\right).\cos\left(\omega_s t + \frac{2\pi}{3}\right)\right\} \quad (21)$$

Table 5 FFT coefficients of equivalent voltage and current phase angle variation in IEEE-14 bus system under asynchronous measurements of voltage and current phasors

Sl. no.	Fault location	Fault type	Δ (α_Δ, β_Δ)	Ψ (α_Ψ, β_Ψ)	Υ_R, Υ_Y, Υ_B	SVM-based classifier	Classification remark
1	branches 2–4, 60 km from bus-2	AG	0.17, 0.49	0.04, 0.02	0.73, 1, 0.99	AC	misclassified
2	branches 4–5, 50 km from bus-4	BG	0.20, 0.56	0.05, 0.01	0.99, 0.68, 1	ABG	misclassified
3	branches 1–2, 70 km from bus-1	CG	0.18, 0.44	0.02, 0.02	1, 0.99, 0.74	AC	misclassified
4	branches 3–4, 20 km from bus-3	AB	0.05, 1.32	0.05, 0.01	0.76, 0.77, 1	ACG	misclassified
5	branches 13–14, 10 km from bus-13	BC	0.01, 0.9	0.06, 0.03	1, 0.84, 0.84	ABG	misclassified
6	branches 6–11, 40 km from bus-6	CA	0.02, 0.69	0.03, 0.02	0.84, 1, 0.85	CAG	misclassified
7	branches 12–13, 90 km from bus-12	ABG	0.11, 0.64	0.05, 0.03	0.79, 0.81, 1	AB	misclassified
8	branches 7–9, 80 km from bus-7	BCG	0.14, 0.80	0.07, 0.04	1, 0.78, 0.72	BC	misclassified
9	branches 4–9, 10 km from bus-4	CAG	0.13, 0.74	0.05, 0.02	0.77, 1, 0.73	CA	misclassified
10	branches 9–10, 30 km from bus-6	ABC	0.11, 0.12	0.07, 0.1	1, 1, 1	AB	misclassified

6 Conclusion

Incorporation of GPS synchronised PMUs have paved the way for advanced real-time protection strategies for emerging SPGs. This paper proposes a real-time fault identification and classification methodology for SPG that can precisely detect and classify any type of fault at any location within SPG. The major contribution of the proposed methodology is that single PMU measurements at any one of the generator buses in the grid are sufficient to detect and classify transmission line fault occurring anywhere in the grid. FFT coefficients extracted from equivalent voltage and current phase angles only at one of the generator buses are utilised for fault identification and classification. The proposed methodology can be utilised for relaying purposes in case of single transmission lines as well as for SPC applications in power grid networks. However, the significance of the fault information from the methodology is for assisting SPC in SPGs for fault detection and classification algorithms to restore the transmission lines at the earliest and to initiate wide-area control actions to maintain system stability against disturbances generated because of occurrence and clearance of faults.

7 References

1 Masoum, A.S., Deilami, S., Moses, P.S., Masoum, M.A.S., Abu-Siada, A.: 'Smart load management of plug-in electric vehicles in distribution and residential networks with charging stations for peak shaving and loss minimisation considering voltage regulation', *IET Gener. Transm. Distrib.*, 2011, **5**, (8), pp. 877–888

2 Garcia-Valle, R., da Silva, L.C.P., Xu, Z., Ostergaard, J.: 'Smart demand for improving short-term voltage control on distribution networks', *IET Gener. Transm. Distrib.*, 2009, **3**, (8), pp. 724–732

3 Klimstra, J., Hotakainen, M.: 'Smart power generation' (Avain Publishers, Helsinki, 2011)

4 Garrity, T.F.: 'Getting smart: innovation and trends for future electric power systems', *IEEE Power Energy Mag.*, 2008, **6**, (2), pp. 38–45

5 Massoud Amin, S., Wollenberg, B.F.: 'Toward a smart grid: power delivery for the 21st century', *IEEE Power Energy Mag.*, 2005, **3**, (5), pp. 34–41

6 Phadke, A.G., Thorp, J.S.: 'Synchronized phasor measurements and their applications' (Power Electronics and Power Systems Series, Springer Publication, New York, 2008)

7 Phadke, A.G., Thorp, J.S., Adamiak, M.G.: 'A new measurement technique for tracking voltage phasors, local system frequency, and rate of change of frequency', *IEEE Trans. Power Appar. Syst.*, 1983, **PAS-102**, (5), pp. 1025–1038

8 Donnelly, M.K., Dagle, J.E., Trudnowski, D.J., Rogers, G.J.: 'Impacts of the distributed utility on transmission system stability', *IEEE Trans. Power Syst.*, 1996, **11**, (2), pp. 741–746

9 Slootweg, J.G., Kling, W.L.: 'Impacts of distributed generation on power system transient stability', *Proc. IEEE Power Eng. Soc. Summer Meet.*, 2002, **2**, pp. 862–867

10 Cecati, C., Citro, C., Siano, P.: 'Combined operations of renewable energy systems and responsive demand in a smart grid', *IEEE Trans. Sustain. Energy*, 2011, **2**, (4), pp. 468–476

11 Gopakumar, P., Jaya bharata Reddy, M., Mohanta, D.K.: 'Letter to the editor: stability concerns in smart grid with emerging renewable energy technologies', *Electr. Power Compon. Syst.*, 2014, **42**, (3–4), pp. 418–425

12 Ma, J., Zhang, P., Fu, H., Bo, B., Dong, Z.: 'Application of phasor measurement unit on locating disturbance source for low-frequency oscillation', *IEEE Trans. Smart Grid*, 2010, **1**, (3), pp. 340–346

13 Seethalekshmi, K., Singh, S.N., Srivastava, S.C.: 'A synchrophasor assisted frequency and voltage stability based load shedding scheme for self-healing of power system', *IEEE Trans. Smart Grid*, 2011, **2**, (2), pp. 221–230

14 Hashiesh, F., Mostafa, H.E., Khatib, A., Helal, I., Mansour, M.M.: 'An intelligent wide area synchrophasor based system for predicting and mitigating transient instabilities', *IEEE Trans. Smart Grid*, 2012, **3**, (2), pp. 645–652

15 Chanda, D., Kishore, N.K., Sinha, A.K.: 'Application of wavelet multiresolution analysis for identification and classification of faults on transmission lines', *Electr. Power Syst. Res.*, 2005, **73**, (3), pp. 323–333

16 Ferrero, A., Sangiovanni, S., Zapitelli, E.: 'A fuzzy set approach to fault type identification in digital relaying', *IEEE Trans. Power Deliv.*, 1995, **10**, (1), pp. 169–175

17 Robertson, D.C., Camps, O.I., Mayer, J.S., Gish, W.: 'Wavelets and electromagnetic power system transients', *IEEE Trans. Power Deliv.*, 1996, **11**, (2), pp. 1050–1058

18 Jaya Bharata Reddy, M., Mohanta, D.K.: 'Adaptive-neuro-fuzzy inference system approach for transmission line fault classification and location incorporating effects of power swings', *IET Gener. Transm. Distrib.*, 2008, **2**, (2), pp. 235–244

19 Bo, Z.Q., Aggarwal, R.K., Johns, A.T., Li, H.Y., Song, Y.H.: 'A new approach to phase selection using fault generated high frequency noise and neural networks', *IEEE Trans. Power Deliv.*, 1997, **12**, (1), pp. 106–113

20 Jaya Bharata Reddy, M., Mohanta, D.K.: 'A wavelet-fuzzy combined approach for classification and location of transmission line faults', *Int. J. Electr. Power Energy Syst.*, 2007, **29**, (9), pp. 669–678

21 Jaya Bharata Reddy, M., Mohanta, D.K.: 'A wavelet-neuro-fuzzy combined approach for digital relaying of transmission line faults', *Electr. Power Compon. Syst.*, 2007, **35**, (12), pp. 1385–1407

22 Lopes, F.V., Santos, W.C., Fernandes, D., Neves, W.L.A., Souza, B.A.: 'An adaptive fault location method for smart distribution and transmission grids'. IEEE PES Conf. on Innovative Smart Grid Technologies (ISGT Latin America), 2011, pp. 1–7

23 Ferraz, R.G., Iurinic, L.U., Filomena, A.D., Bretas, A.S.: 'Park's transformation analytical approach of transient signal analysis for power systems', North American Power Symp. (NAPS), 9–11 September 2012, pp. 1–6

24 Demetrios, A.T., McLaren, P., Alexander, G., *et al.*: 'Mathematical models for current, voltage, and coupling capacitor voltage transformers', *IEEE Trans. Power Deliv.*, 2000, **15**, (1), pp. 62–72

25 Kundur, P.: 'Power system stability and control' (Tata McGraw-Hill Education Pvt. Ltd., New Delhi, 2012)

26 Ravikumar, B., Thukaram, D., Khincha, H.P.: 'Comparison of multiclass SVM classification methods to use in a supportive system for distance relay coordination', *IEEE Trans. Power Deliv.*, 2010, **25**, (3), pp. 1296–1305

doi: 10.1049/iet-gtd.2014.0024

27 Kalyani, S., Shanti Swarup, K.: 'Classification and assessment of power system security using multiclass SVM', *IEEE Trans. Syst. Man Cybern. C, Appl. Rev.*, 2011, **41**, (5), pp. 753–758
28 Dash, P.K., Samantaray, S.R., Panda, G.: 'Fault classification and section identification of an advanced series-compensated transmission line using support vector machine', *IEEE Trans. Power Deliv.*, 2007, **22**, (1), pp. 67–73
29 Vapnik, V.: 'Statistical learning theory' (Wiley, New York, 1998)
30 Hsu, C.W., Lin, C.J.: 'A comparison of methods for multiclass support vector machines', *IEEE Trans. Neural Netw.*, 2002, **13**, (2), pp. 415–425
31 Vapnik, V.N.: 'The nature of statistical learning theory' (Springer-Verlag, New York, 1995)
32 Chang, C.C., Lin, C.J.: 'LIBSVM: a library for support vector machines', *ACM Trans. Intell. Syst. Technol.*, 2011, **2**, pp. 27:1–27:27. Software available at http://www.csie.ntu.edu.tw/~cjlin/libsvm
33 Seyedtabaii, S.: 'Improvement in the performance of neural network-based power transmission line fault classifiers', *IET Gener. Transm. Distrib.*, 2012, **6**, (3), pp. 731–737
34 Bogdan, K., Bruce, C., Jeff, M.: 'Phase selection for single-pole tripping: weak infeed conditions and cross-country faults'. 27th Annual Western Protective Relay Conf., Spokane, 2000, pp. 1–19, Available at http://www.store.gedigitalenergy.com/faq/Documents/Alps/GER-3997.pdf